Petroleum and Coal

Article **Open Access**

Performance Evaluation and Optimization of Advanced Cyclone System for Palm Waste Induced Flue Gas

Naresh K. Uthama Kumaran[1], Ho Cheng How[2], Girma T. Chala[3*], Poon Han Wong[1], Edmund De Alwis[1]*

[1] *Boilermech Sdn. Bhd., Lot 875, Jalan Subang 8, Taman Perindustrian Subang, 47620 Subang Jaya, Selangor, Malaysia*
[2] *Department of Mechanical. Materials & Manufacturing Engineering, University of Nottingham Malaysia, Jalan Broga 43500 Semenyih, Selangor, Malaysia*
[3] *International College of Engineering and Management, P.O. Box 2511, C.P.O Seeb 111, Muscat, Oman*

Received June 16, 2021; Accepted January 14, 2022

Abstract

The performance of a cyclone is primarily determined by three key parameters; namely inlet velocity, pressure drop across inlet and outlet, and particle collection efficiency. To achieve optimal design and development cost, it is vital to have an accurate prediction of pressure drop and particle collection efficiency of the cyclone in response to the variation of inlet velocities. The present study focuses on the design of a serial-configured multi-cyclones system that is capable of reducing the particle emission of the flue gas from 4000 mg/Nm^3 to 150 mg/Nm^3 in a palm waste-fueled boiler system. Optimization of inlet velocity on individual cyclones is performed within the serial-configured multi-cyclones system using a combined computational fluid dynamic simulation (CFD) and the Stairmands's high-efficiency cyclone model-based design analysis. To further improve the accuracy of the design analysis and the CFD simulation, the flue gas at the inlet of the serial-configured multi-cyclones system was sampled, and the distribution of particle size was analyzed. It was observed that an inlet velocity of 20 m/s was found to be optimum, which was later used to determine the total number of cyclones in the design of the serial-configured multi-cyclones system. The use of the newly designed outlet ducting of rectangular shape produces the desired pressure gradient with the presence of negative draft along the outlet ducting.

Keywords: *Cyclone; Palm waste; Flue gas; Performance; Optimization.*

1. Introduction

Gas or liquid flow separation by utilizing a method of centrifugal force is best achieved by the usage of devices such as cyclones [1-2]. This inertial-based separating device is used as the method of pollution control in industries [3], and it is chosen amongst other methods for dust removal mainly due to its high efficiency performance and its cost effectiveness [4]. In a cyclone, particles-contaminated air is fed into a chamber of the cyclone. The chamber allows the formation of a spinning vortex that exhausts the clean gas and leaves behind the solid particles to be dispersed along its wall [5]. While the lighter weight particles have the tendency to get attracted to the spinning vortex, and travel upwards to the outlet of the cyclone, the heavier particles continue their path towards the dust collector at the bottom of the cyclone [6].

There are many factors affecting the performance of the cyclone; among which the velocity of the particles that travelled along the wall of the cyclone [7], and the particles residence time are the dominant factors [8]. The particle residence time defines the time required for the particle to flow through the length of the cyclone to the dust collector [9]. The residence time affects the performance of the cyclone as the slower the time the lesser is the efficiency. In fact, roughness of the wall of the chamber, particle density, and inlet velocity are also found to affect the particle residence time [10].

The performance of the cyclone can be analyzed by the amount of energy used for the movement of the particles within the cyclone, as well as based on its efficiency curve [11]. It could be seen that the centrifugal force is directly dependent on the increase of inlet velocity. Higher inlet velocity of the cyclone provides a higher chance for the particles to exit the cyclone [12]. Pressure drop of the cyclone is another parameter that has dependency on the change in inlet velocity. It was reported that the increase in inlet velocity resulted in an exponential increase in pressure drop, as well as an increase in the collection efficiency of the cyclone [13-14]. It is important to note that the increase in inlet velocity requires less cyclones in a multi-cyclones system to accommodate the gas flow rate.

Though there are many research available on the cyclone, there are limited studies when it comes to the cyclones system for palm waste-induced flue gas, especially for the advanced serial-configured multi-cyclones system. Such an investigative study is even more important with recent tightening of the particle emission limit from 400mg/Nm^3 to 150mg/Nm^3 by the Malaysian Department of Environment. As a measure to fulfill the requirement from the regulatory body, as well as to commit to a cleaner environment, the present study focuses on the performance investigation and optimization of the design of the advanced multi-cyclones system using computational fluid dynamic simulation. To further improve the accuracy of the simulation, the flue gas at the inlet of the multi-cyclones system was sampled, and the distribution of particle size was used to validate the simulation results.

2.Methodology

2.1. Mathematical model

There are various models used in the design of cyclone, such as Barth *et al.* [15], Leith and Licht [16], Coker [17], Mothes *et al.* [18], Chen and Shi [19] and Moore and McFarland [20]. The model adopted for this study is the Stairmand model. This model is widely used in the industry and its design is readily available. There are two types of design for the Stairmand model; namely high efficiency, and high gas rate cyclones. The standard cyclone dimension as per Stairmand high efficiency model was chosen in this case.

The inlet velocities were varied at 15m/s, 17.5m/s 20m/s, 22.5m/s and 25m/s to attain the most optimum result with respect to the pressure drop, collection efficiency, and the total number of cyclones needed for the serial-configured multi-cyclones system. This is done by collecting flue gas samples at the inlet of the serial-configured multi-cyclones system where the number of particles in one cubic meter volume is quantified in terms of mass percentage in various ranges of particle size. Using the scaling factor, the figure of collection efficiency can then be changed to other cyclone sizes based on equation (1) [21].

$$D_2 = [(DC_2/DC_1)^3 \times Q_1/Q_2 \times \Delta\rho_1/\Delta\rho_2 \times \mu_2/\mu_1]^{1/2} \quad (1)$$

where, D_2= mean diameter of the particle separated in the proposed design, at the chosen separating efficiency; DC_2= diameter of the standard cyclone = 8 inches (203mm); DC_1= diameter of the proposed cyclone, mm; Q_1= standard flow rate (for high efficiency design = 223 m^3/hour,); Q_2= proposed flow rte, m^3/hour; $\Delta\rho_1$= solid-fluid density difference in standard conditions; $\Delta\rho_2$= density difference in the proposed design; μ_1= test fluid viscosity (air at 1 atm, 200^{o}C) = 0.018 mNs/m^2; μ_2= viscosity of proposed fluid,

The equation above is used to find the scaling factor. The collection efficiency curve could be shifted according to the intended size from the scaling factor. As for the pressure drop in a cyclone, the formula used to calculate is given in equation (2) [21].

$$\Delta P = \rho_f/203 \{u_1^2 [1 + 2\varphi^2 (2r_1/r_e-1)] + 2u_2^2\} \quad (2)$$

where, ΔP = cyclone pressure drop, millibar; ρ_f = gas density, kg/m^{3,}; u_1= inlet duct velocity, m/s; u_2= exit duct velocity, m/s; r_1= radius of circle to which the centerline of the inlet is tangential, m; r_e= radius of the exit pipe, m,φ= factor from Figure 1 where Ψ= parameter in Figure 1, given by $\Psi=F_c A_s/A_1$; F_c = friction factor, taken as 0.005 for gasses; A_s= surface area of cyclone exposed to spinning fluid, m^2; A_1= area of inlet duct, m^2.

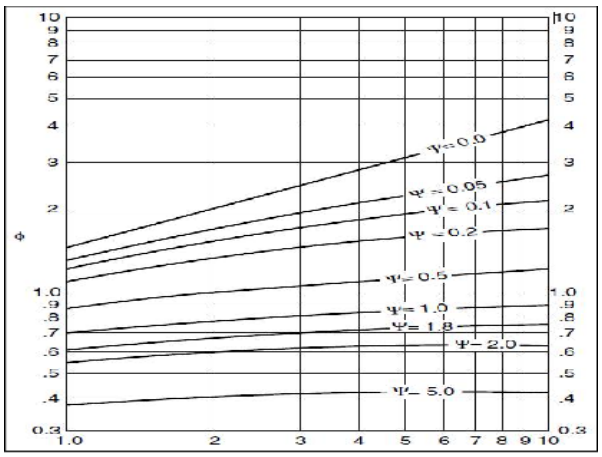

Figure 1. Cyclone pressure drop factor (Gopani and Bhargava[21])

The pressure drop across the cyclone is mainly created by entry and exit losses [21]. Moreover, the friction and kinetic energy losses in the cyclone could also cause pressure drop across the cyclone. Using Stairmand model [20], a benchmark value for the simulation was attained. Even though the theoretical values gained would not be as precise; however, a guideline would be achieved when referred with the simulation results. The number of cyclones required was calculated using simple theory of discharge, based on an inlet flow of 62,000 cubic feet per minute and a constant inlet area of the cyclone.

2.2. CFD simulation

ANSYS-FLUENT workbench is used to carry out the simulation for a single cyclone, and row of 12 serial-configured cyclones with a common inlet and a common outlet ducting. The single cyclone simulation is done with Reynolds Stress Model (RSM) and Discrete Particle Model (DPM); whereas for the serial-configured cyclones, only the RSM is performed [22].

Description of the strong swirling gas-solid flow was done by the RSM where anisotropy became the base of building this model. Referring to the experimental results, it was seen that certain characteristics agreed such as the pressure drop and flow characteristics. By ignoring the particle-particle collision, the object is taken as a single particle by DPM. Inaccuracy occurs in DPM only when the particle size diameter was found to be larger than 0.1mm [23]. The mass and momentum conservation law are given by:

$$\frac{\partial(\alpha\rho_f)}{\partial t} + \Delta \cdot (\alpha\rho_f u_f) = 0 \quad (3)$$

$$\frac{\partial(\alpha\rho_f u_f)}{\partial t} + \Delta \cdot (\alpha\rho_f u_f u_f) = -\alpha\Delta p + \alpha\Delta \cdot \tau - S_f + \alpha\rho_f g \quad (4)$$

where, α, ρ_f, u_f, τ and S_f represent gas phase volume, gas density, gas velocity, viscosity stress tensor and mean force in the computational cells, respectively [23].

To describe the strong swirling gas flow in a cyclone, a Reynolds Stress Turbulence Model was adopted.

$$U_k\frac{\partial(\bar{u_i'}\bar{u_j'})}{\partial x_k} = D_{ij} + P_{ij} + \varphi_{ij} - \epsilon_{ij} \quad (5)$$

$$D_{ij} = -\frac{\partial}{\partial x_k}\left(\frac{\mu_t}{\sigma_k}\frac{\partial \bar{u_i'}\bar{u_j'}}{\partial x_k}\right) \quad (6)$$

$$P_{ij} = -\rho\left(\bar{u_i'}\bar{u_k'}\frac{\partial u_j}{\partial x_k} + \bar{u_j'}\bar{u_k'}\frac{\partial u_i}{\partial x_k}\right) \quad (7)$$

$$\varphi_{ij} = P\left(\frac{\partial \bar{u_i'}}{\partial x_j} + \frac{\partial \bar{u_j'}}{\partial x_i}\right) \quad (8)$$

$$\epsilon_{ij} = 2\mu\frac{\partial \bar{u_i'}}{\partial x_j}\frac{\partial \bar{u_j'}}{\partial x_i} \quad (9)$$

where the Cartesian coordinates system are represented by i, j and k; the diffusion term, stress generation term, dispersion term and turbulence viscosity are represented by D_{ij}, P_{ij} and ϵ_{ij} respectively, and the velocity fluctuations are represented by $u`_i$, $u`_j$ and $u`_k$ respectively [23].

The trajectory of a discrete phase particle is predicted by ANSYS-FLUENT via a Lagrangian reference frame whereby the force balance projected on the particle is integrated. The particle force and particle inertia equate to the force balance equation as shown below (Cartesian coordinates x direction)

$$\frac{du_p}{dt} = F_D(u - u_p) + \frac{g_x(p_p - p)}{p_p} + F_x \quad (10)$$

where the drag force per unit particle mass is $F_D(u - u_p)$, u as fluid phase velocity, u_p is the particle velocity [24].

$$F_D = \frac{18\mu}{d_P^2 \rho_P C_c} \frac{C_D Re}{24} \quad (11)$$

The parameters above denote that μ is the fluids molecular viscosity, ρ is the fluid density, ρ_p is the density of the particle, and d_p is the particle diameter. Re denotes Reynolds number, which is given as below.

$$Re \equiv \frac{\rho d_p |u_p - u|}{\mu} \quad (12)$$

The drag coefficient, C_D, is given as $C_D = a_1 + \frac{a_2}{Re} + \frac{a_3}{Re^2}$

where a_1, a_2, and a_3 are constants for smooth spherical particles over several ranges of Re.

$$C_D = \frac{24}{Re}(1 + b_1 Re^{b_2}) + \frac{b_3 Re}{b_4 + Re} \quad (13)$$

where

$b_1 = \exp(2.3288 - 6.4581\varphi + 2.4486\varphi^2)$

$b_2 = 0.0964 + 0.5565\varphi$

$b_3 = \exp(4.905 - 13.8944\varphi + 18.4222\varphi^2 - 10.2599\varphi^3)$

$b_4 = \exp(1.4681 + 12.2584\varphi - 20.7322\varphi^2 + 15.8855\varphi^3)$(19.2-6)

which are taken from Haider and Levenspiel [24]. The shape factor, φ, is

$$\varphi = \frac{s}{S} \quad (14)$$

where s stands for the surface area of a sphere with the same volume as the particle and S stands for the actual surface area of the particle.

$$F_D = \frac{18\mu}{d_P^2 \rho_P C_c} \quad (15)$$

The equation is for sub-micron particles, Stokes' drag law. In this case, F_D is defined as the above. The factor C_c is the Cunningham correction to Stokes' drag law, which is given as follows:

$$C_c = 1 + \frac{2\lambda}{d_p}\left(1.257 + 0.4e^{-\left(\frac{1.1 d_p}{2\lambda}\right)}\right) \quad (16)$$

where the molecular mean free path is noted by λ.

It is also possible to get a high Mach number drag law by simply altering the Mach number greater than 0.4 or Reynolds number greater than 20. For models that involve discrete phase droplet breakup there is an option for dynamic drag law.

2.2.1. Boundary conditions

An inlet velocity boundary was selected at the cyclone inlet. The outflow was set at the outlet boundary, and the no-slip boundary conditions were implied to the other boundaries. All the simulations run with the time step at 1e-04 for the gas flow. The Semi-Implicit Method for Pressure-Linked Equations (SIMPLE) was set for the pressure-velocity coupling algorithm. Second Order Upwind was selected as a discretization for momentum whereas PRESTO! (Pressure Staggered Option) was set for pressure. Second Order Upwind scheme was implied for the turbulent kinetic energy, turbulent dissipation rate and Reynolds stress.

An inlet velocity of 15 m/s, 17.5 m/s, 20 m/s, 22.5 m/s and 25m/s were used, and the gauge pressure was zero with reference to the atmospheric pressure. The flue gas exiting the boiler is of high temperature. Gas density was considered to be 0.585 kg/m^3, gas viscosity as 2.4x10^{-5} kg/m.s and operating temperature was taken to be 513K.

As for DPM, the inlet and wall boundary were set to be "reflect" and the gas outlet was set to be "escape" and ash outlet was set to be "trap". Other than that, the solid loading was given the same inlet velocity as the gas flow. The particle shape was assumed to be spherical and the particles were scattered evenly around the inlet boundary. Moreover, the particle chosen was solid ash.

The simulation process started off with the meshing of the inner volume of the single cyclone. The mesh type used was a tetrahedral mesh. A study on three different cell numbers was conducted to justify that the cell number is independent from the pressure drop. Table 1 shows the pressure drop and the percentage difference for different mesh sizes.

Table 1. Pressure drop across cyclone with different mesh size

Cell number	Pressure drop (Pa)	% Difference
270000	401	
3700000	420	4.5
470000	409	

The simulation results were compared with the mathematical model for all velocities. This acts as a verification factor to validate the simulation results, and thus the optimal velocity was identified to proceed to the serial-configured cyclones.

For the cyclones arranged in the series configuration, the same tests were conducted with higher cell numbers, ranging from 1 million to 10 million cells. Pressure drop for the series configured cyclones is depicted in Table 2. In this case, the pressure drop difference was found to be less than 7%, and this is sufficient to justify the independence of the cell number and pressure drop within the range of this study [23].

Table 2. Pressure drop in series configurated cyclones with different mesh size

Cell number	Pressure drop (Pa)	% Difference
1000000	420	
5000000	452	6.6
10000000	448	

3. Results and discussion

3.1. Mathematical model

The collection efficiency for various ranges of particles size at each inlet velocity was tabulated based on the actual flue gas sample that collected at the inlet of the cyclone, before the total collection efficiency was summarized. Table 3 shows the pressure drop across the inlet and the outlet, and the total collection efficiency of the cyclone for each inlet velocity.

Table 3. Pressure drop and total collection efficiency of the cyclone for each inlet velocity

Inlet velocity (m/s)	Pressure drop, ΔP (Pa)	Total collection efficiency (%)
15	385.95	58.24
17.5	525.39	59.23
20	687.24	60.06
22.5	871.5	60.78
25	1075.68	61.40

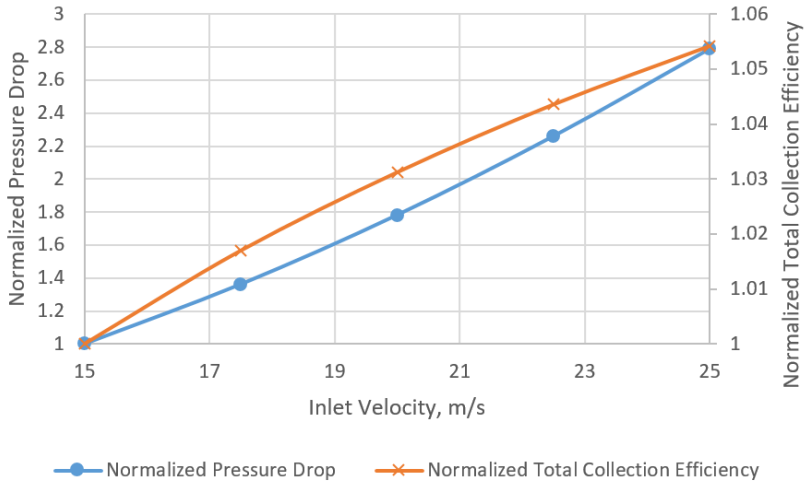

Figure 2. The effect of inlet velocity on pressure drop and total collection efficiency (based on mathematical model)

To further investigate the effect of inlet velocity, both the pressure drop and the total collection efficiency were normalized, and plotted against the inlet velocity, as shown in Figure 2. The effect of inlet velocity on pressure drop was obviously significant, but not the total collection efficiency. By increasing the inlet velocity from 15m/s to 25m/s, the increment seen in pressure drop was as high as 2.8 times, but the total collection efficiency was merely increased by 5.4%.

3.2. CFD simulation for a single cyclone

Based on the CFD simulation, the pressure values at the inlet, outlet, and ash outlet of the cyclone were recorded, and plotted against its inlet velocity in Figure 3. It was noted that the normalized pressure at the inlet, outlet, and ash outlet of the cyclone generally increased with inlet velocity. However, a slightly different trend for ash outlet pressure was observed, whereby the increment of pressure appeared to saturate at the velocity of 22.5m/s.

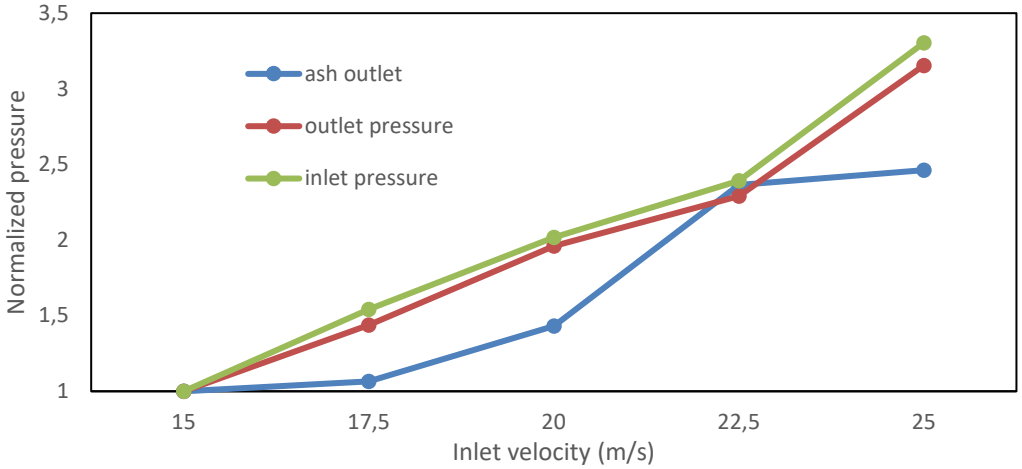

Figure 3. The effect of inlet velocity on inlet pressure, outlet pressure, and ash outlet pressure (based on CFD simulation)

By plotting the weight distribution of various particles sizes from the actual flue gas sample that collected at the inlet of the cyclone, Figure 4, the removal of particles within the range of 1μm to 12μm deserved higher attention in determining the optimum inlet velocity of the cyclone. Therefore, a set of particles of 1.11μm, 4.06μm, 7.77μm and 10.75μm were selected for the simulation of the particle tracking using DPM, with inlet velocities varied from 15m/s, 17.5m/s, 20m/s, 22.5m/s and 25m/s.

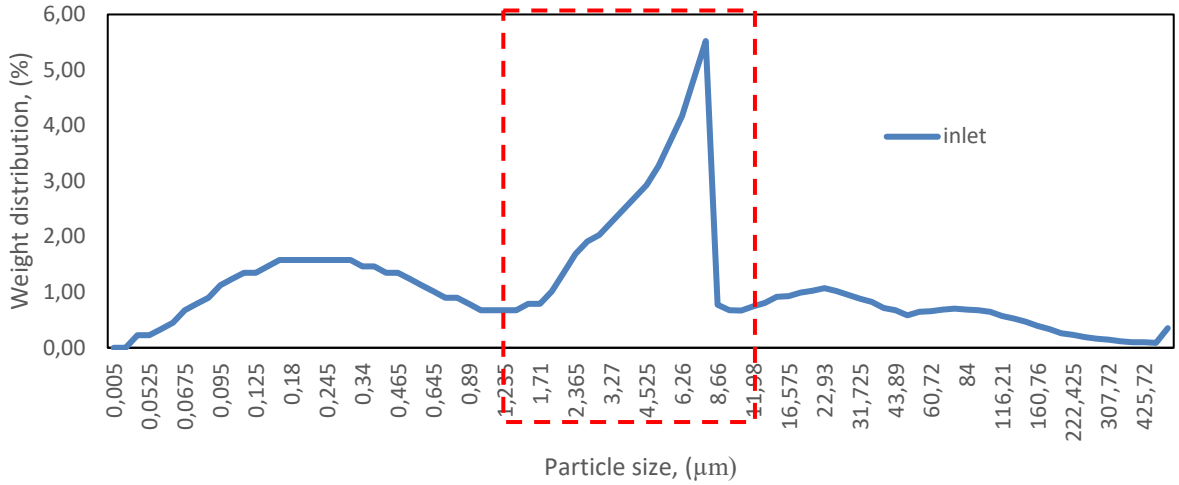

Figure 4. Percentage weight distribution against various particles sizes

It can be seen from Table 4 that the maximum collection efficiency is achieved for particle size of 10.75μm across all velocities, whereas the minimum efficiency of 79% to 86% was witnessed for particle size of 1.11μm. However, an increasing trend of the efficiency was noticed amongst all the inlet velocities with the increase of particle size, as shown in Figure 5. Higher inlet velocity causes greater centrifugal force which makes the particle move towards the wall faster which in turn increases the collection efficiency. Other than that, the increase in efficiency across the velocities is generally due to the increase in pressure gradient at the cyclone's ash outlet. This results in the formation of vortexes in the cyclone, thus giving rise to higher particle collection efficiency.

Table 4. Collection efficiency of different particle size for different velocities

Inlet velocity (m/s)	Collection efficiency (%)			
	1.11μm	4.06μm	7.77μm	10.75μm
15	78.66	95.28	99.31	100
17.5	79.84	95.58	99.61	100
20	80.56	97.22	100	100
22.5	83	97.64	100	100
25	85.83	98.43	100	100

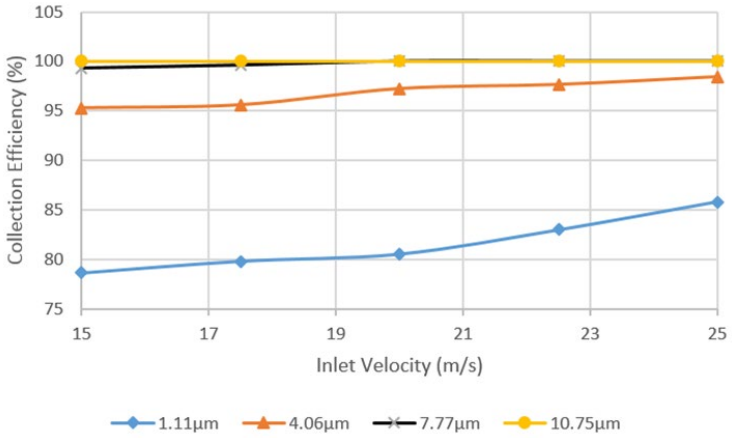

Figure 5. The effect of inlet velocity on collection efficiency for different particles size

3.3. Results comparison between mathematical model and CFD simulation of a single cyclone

The pressure drop across the inlet and the outlet of the single cyclone that was obtained based on the mathematical model and the CFD simulation was compared. The results are shown in a normalized scale to highlight a similar trend in both cases.

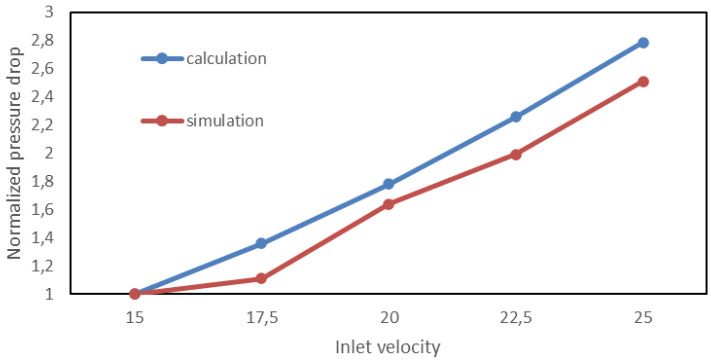

Figure 6. Normalized scale of pressure drop across inlet and outlet of the cyclone

As seen in Figure 6, the difference in both pressure drops is consistent, and the value is increasing with velocity. It can also be seen that the mathematical model values are

consistently higher than the values of CFD simulation. This is mainly due to the reason that only the gas flow was considered in the simulation, whereas the gas flow with the addition of particle tracking was considered in the mathematical model. It is suggested that the dense particles cause the gas flow to have a higher pressure drop [25].

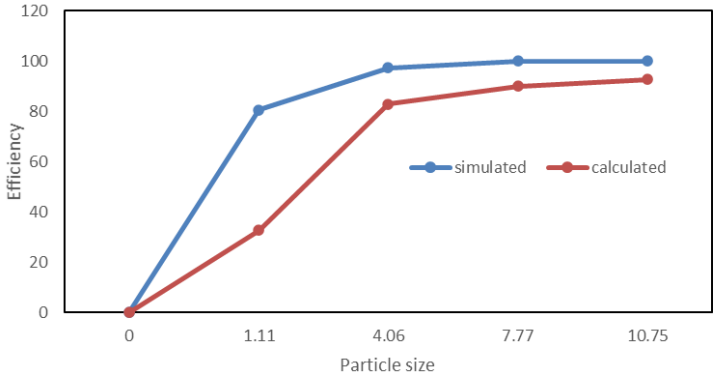

Figure 7. Cyclone efficiency curve

Figure 7 shows the comparison of the collection efficiency curve for the simulated and calculated results at inlet velocity of 20m/s. The reason for taking this inlet velocity as it is the median value of the range of inlet velocities investigated. It is observed that the efficiency increased exponentially with particle size, and the trends appear to be the same for the results that attained in both the calculated and simulated approaches. This proves that the values obtained in simulation are in good agreement with that from the model.

Based on the observation, larger particles are generally heavier, and easier to be collected; whereas smaller and lighter particles are easily escaped through the outlet. Figure 7 shows that both methods show the same trend for 1.11μm with a steep drop in the calculated value. This is because for the simulated values, particle collision and wall attrition are not in the consideration [23]. Moreover, only a particular particle size is used in the simulation for the entire flow.

Table 5 shows the comparison of pressure drop and collection efficiency using the simulation results. The selection of the optimum inlet velocity requires a low pressure drop for better performance, and high collection efficiency for achieving the intended outcome by using the least number of cyclones for a smaller foot-print of the advanced cyclone system. From these assessments a conclusion was made that the best inlet velocity that accommodates for all the criteria is 20m/s.

Table 5. Comparison of 3 key parameters for various velocities

Inlet velocity (m/s)	Pressure drop, ΔP (Pa)	Collection efficiency (%) @4.06μm
15	202.94	95.28
17.5	312.71	95.58
20	409.50	97.22
22.5	485.64	97.64
25	670.54	98.43

3.4. CFD simulation for serial-configured cyclones

With a proper understanding of the optimum performance of a single cyclone, CFD simulation of an array of twelve serial-configured cyclones was carried out to optimize the design of the ducting system that consists of a common inlet ducting, and a common outlet ducting. In this case, the velocity of the gas flow in the common inlet ducting was set to 20m/s as it was deducted to be the optimum value for a single cyclone. The results from the simulation were analyzed for various ducting designs, as described in the following cases A, B, and C.

3.4.1. Case A: A common ducting system with no partition at the inlet ducting

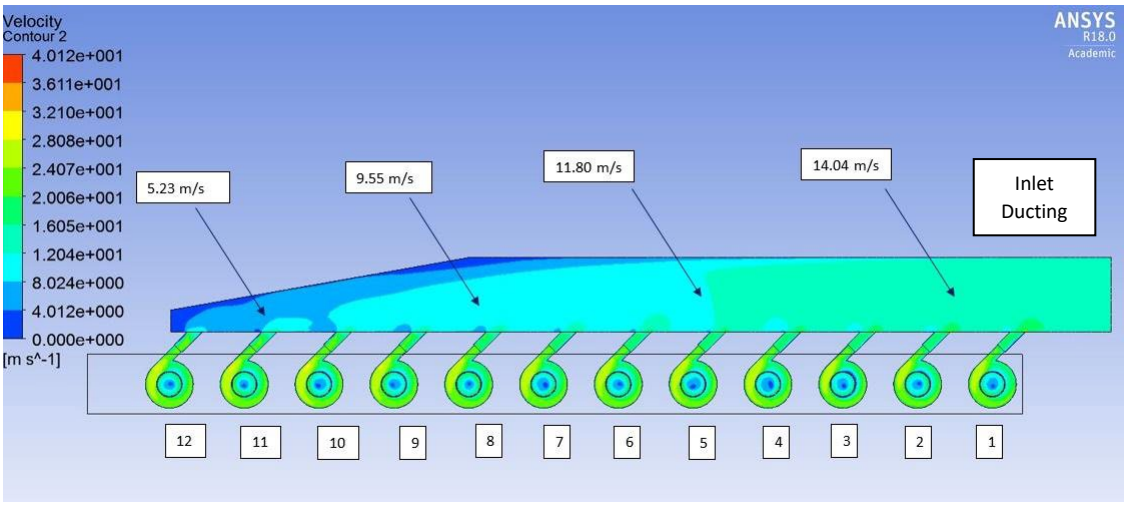

(a)

Figure 8. Case A - (a) Top view of the inlet ducting

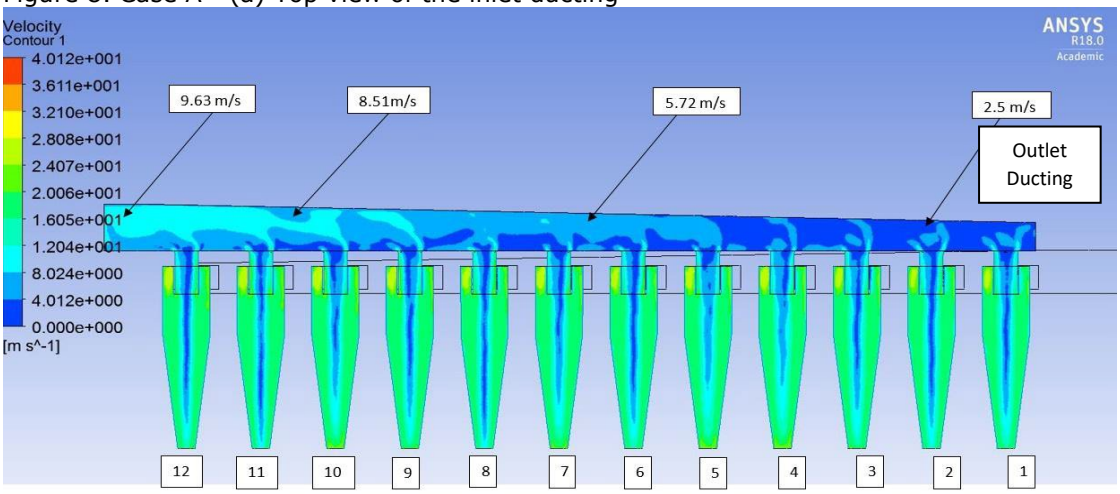

(b)

Figure 8. Case A (b) Side view of the outlet ducting

Figure 8 shows the simulation results of the serial-configured cyclones system in the common ducting system. In Figure 8(a) the distribution of flue gas was uneven in the inlet ducting; whereby the flue gas velocity was found to reduce from 15m/s at the leading edge of the ducting to 5.23m/s at its trailing edge. Figure 8(b) shows the velocity distribution of the serial-configured cyclones and their common outlet ducting. The velocity distribution in the outlet ducting revealed very poor uniformity, especially for cyclones 1, 2, 3 and 4. This allows the particles to be trapped in the outlet ducting and results in re-entry of these trapped particles into the cyclones. Besides, these trapped particles could also lead to clogging issues which required frequent maintenance work.

Figure 9 shows the inlet velocities of these twelve serial-configured cyclones. The velocities obtained across those cyclones were very high. The pressure drop was also obtained by subtracting the pressures at the entry point of the inlet ducting with that of the exit point of the outlet ducting. As a result, the pressure drop was 375.37Pa which was lower than the measured single cyclone value of 419Pa.

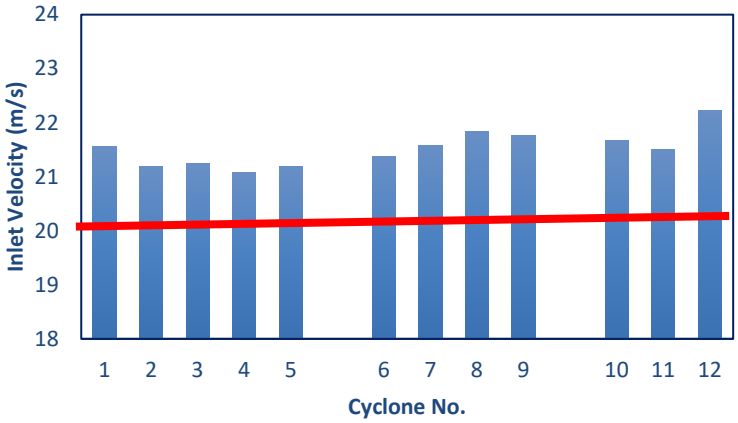

Figure 9. Inlet velocities of cyclones (Case A)

3.4.2. Case B: A common ducting system with partition at the inlet ducting

In this case, two baffle plates were added to the inlet ducting to segregate the inlet ducting into three zones to reduce the inlet velocity of the cyclones, as illustrated in Figure 10(a). The flow of flue gas diverted to cyclones 1-5 for zone 1, cyclones 6-9 for zone 2, and cyclones 10-12 for zone 3.

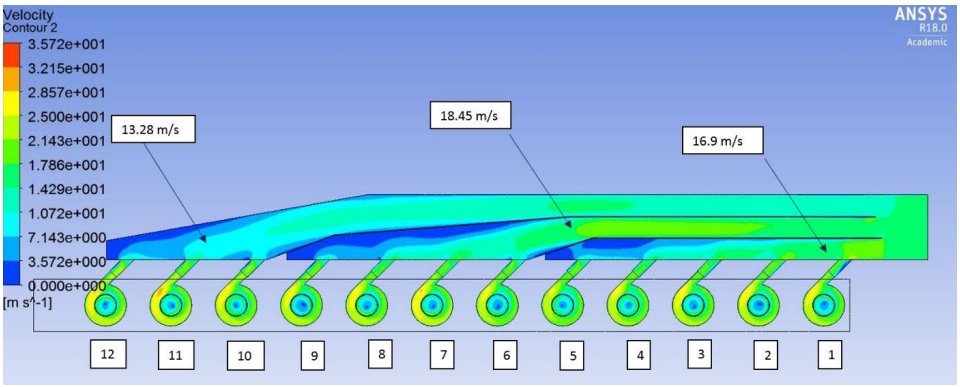

(a)

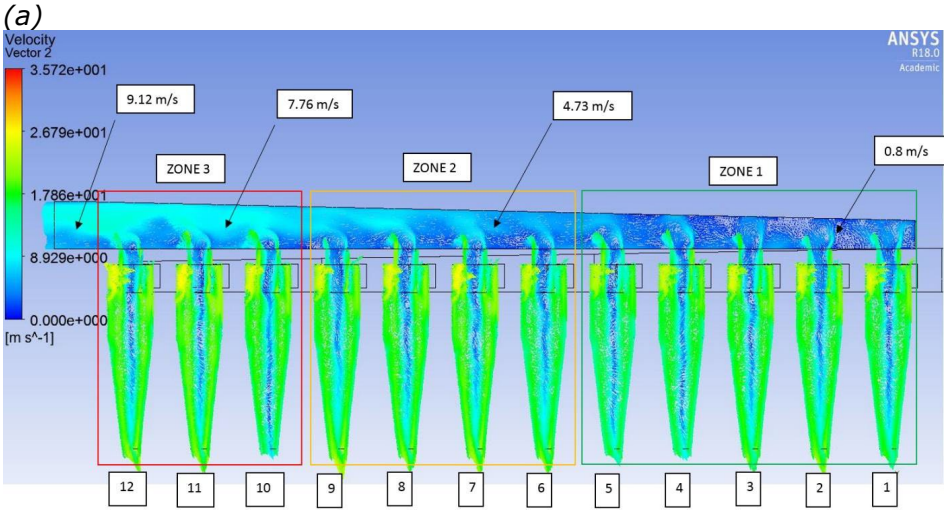

(b)

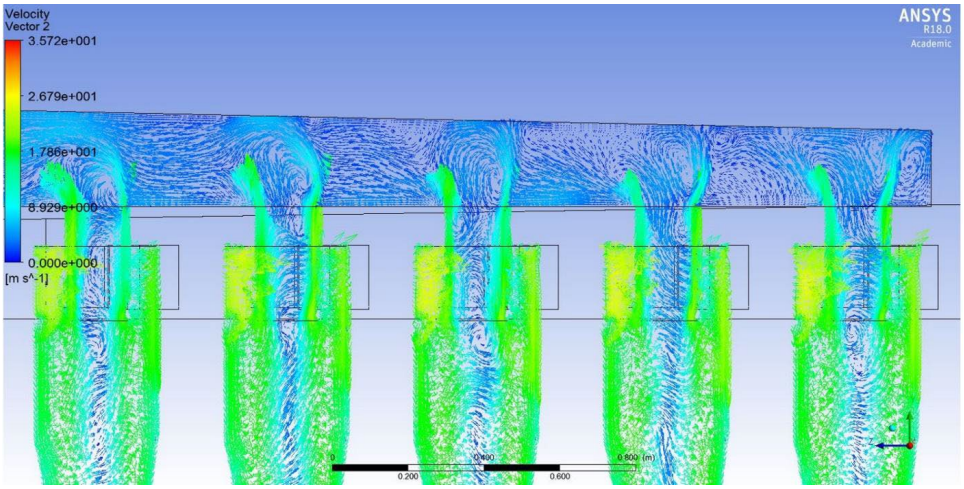

(c)

Figure 10. Effects of partition at inlet ducting, (a) Top view, (b) Side view and (c) Vortex formation at inlet ducting

The partition caused formation of vortex in all three zones could be seen clearly in Figure 10(c). The vortex causes the particles to be held back in inlet ducting that may cause clogging in the long run. Figure 10(b) reveals the improvement in flow distribution in the outlet ducting as compared to the model in Case A.

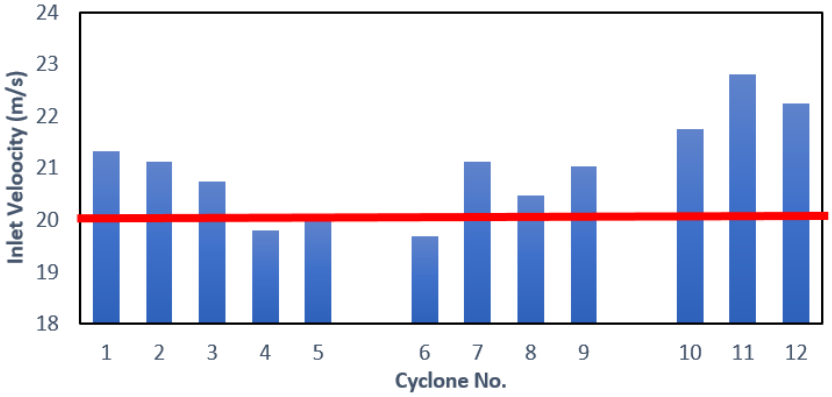

Figure 11. Inlet velocities of cyclones (Case B)

As compared with Figure 9 in Case A, Figure 11 for Case B clearly shows significant variation in inlet velocities across all the twelve cyclones. This indicates poor uniformity in performance in these twelve cyclones. For example, the 6th cyclone in comparison has a very low inlet velocity due to high vortex formation. The pressure drop for this model was 406.16Pa, which was higher than Case A. However, there were a few problems witnessed in this model such as vortex formation and higher variation of inlet velocities.

3.4.3. Case C: A common ducting system with rectangular outlet ducting

Since the inlet ducting was of sufficient flow as evident in Case B, no further optimization was made in the design of the inlet ducting for the Case C. Instead, higher emphasis was focused on the flow of outlet ducting, inlet velocity of cyclones and pressure drop. In this case, the outlet ducting design was modified from a gradually-reduced cross-sectional area to become a uniform rectangular area throughout the whole length of the ducting. Figure 12(a) shows an evenly distributed flow at the inlet ducting. Although zone 2 shows a higher velocity of flue gas, the variation among the zones were not vastly different. This indicates that all the cyclones would be operating around the optimum inlet velocity of 20m/s, as illustrated in Figure 13.

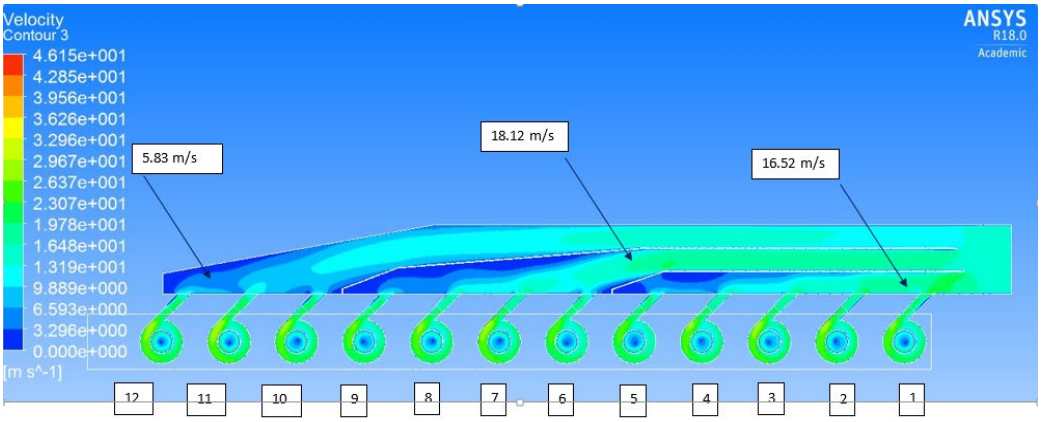

(a)

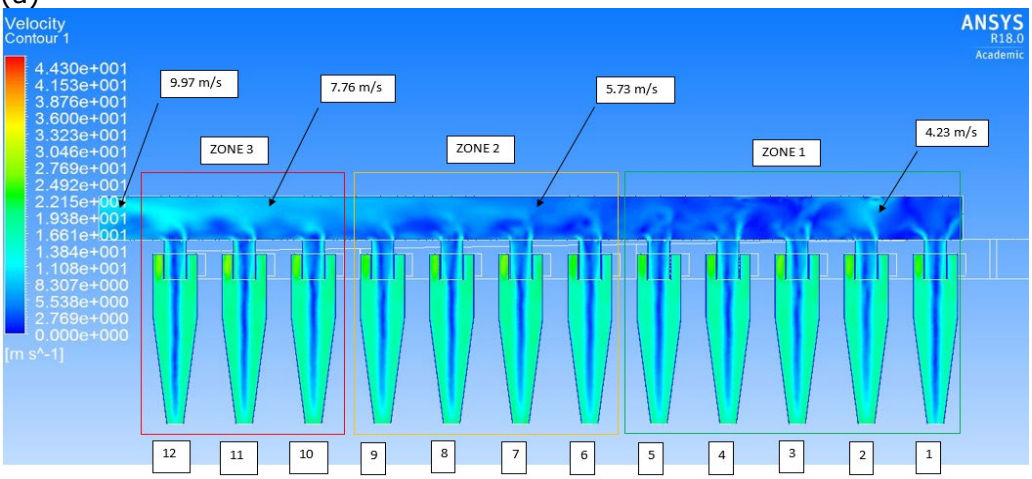

(b)

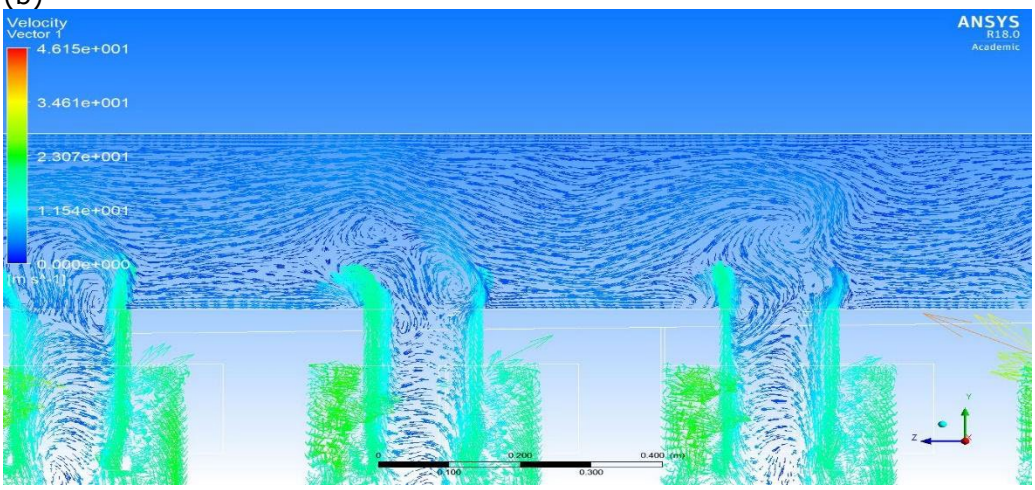

(c)

Figure 12. Effects of rectangular outlet ducting, (a) Top view, (b) Side view and (c) Vortex formation for outlet ducting

It can be seen from Figure 12(b) that the flow of inlet velocity is well distributed as the first three cyclones outlets attained an average velocity of 4.23 m/s in the outlet ducting. The trailing edge of the outlet ducting achieved a velocity of 9.97m/s. In Figure 12(c), the formation of vortex at the outlet ducting was very minimal. This shows that rectangular outlet

ducting provides a viable solution as it minimizes the vortex formation problem, and results in more uniformly distributed gas flow.

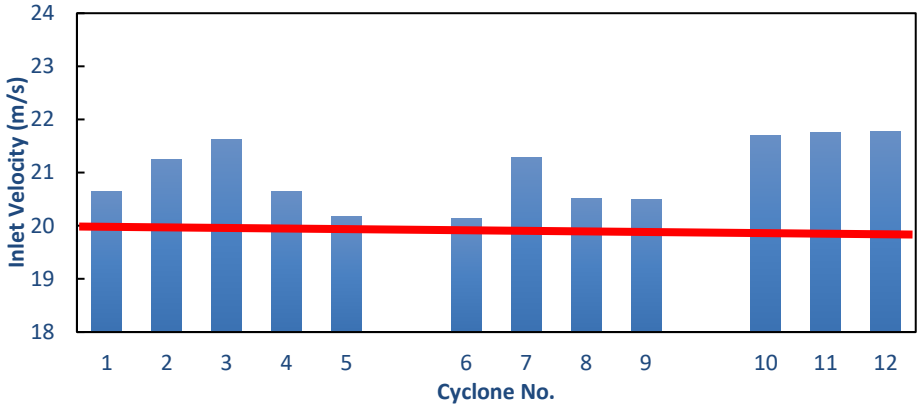

Figure 13. Inlet velocities of cyclones (Case C)

Based on Figure 13, it is seen that the inlet velocity flow is of the best amongst the other cases. The flow is uniformly distributed without having many peaks or lows. However, cyclones in zone 3 had a higher range of velocity across all cyclones. The pressure drop attained was 380.25Pa.

Figure 14 illustrates the outlet ducting pressure distribution of Case B and Case C. Case B shows a negative draft at the zone around cyclones 8 to 12, while a positive draft is observed at the zone around cyclones 1 to 7, Figure 14(a). The negative draft indicates a natural flow gradient for the gas to exit the outlet ducting. However, the positive draft opposes the gas flow, and a lower pressure gradient prevents the gas from exiting the outlet ducting. Such an issue could be avoided in Case C with the presence of negative draft along the whole outlet ducting, Figure 14(b).

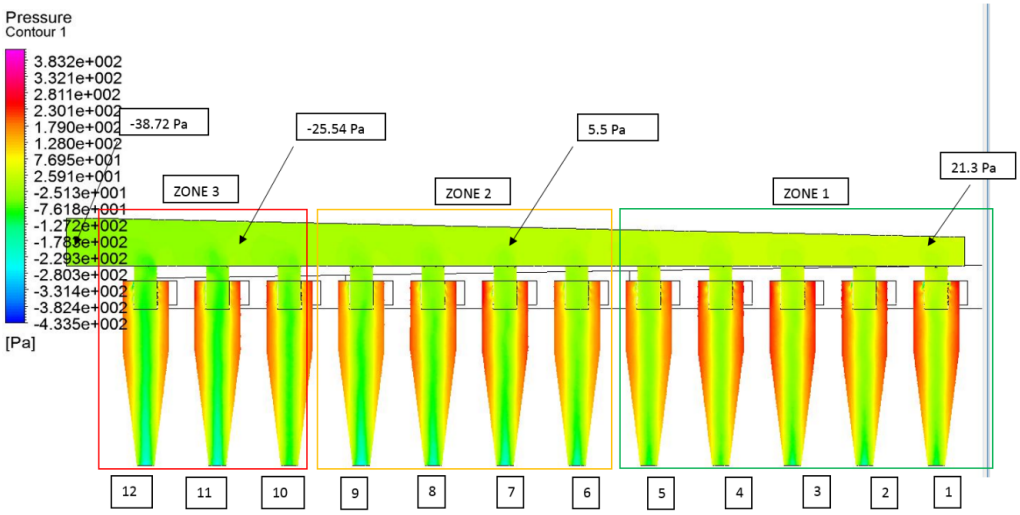

(a)

Figure 14. (a) Side view pressure distribution of Case B

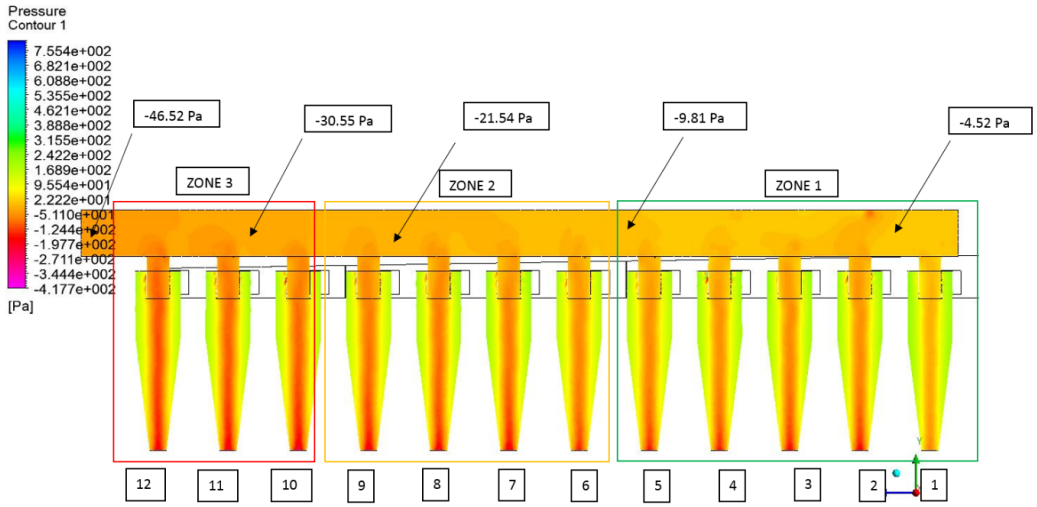

(b)

Figure 14. (b) Side view pressure distribution of Case C

4. Conclusion

A study on performance evaluation and optimization of advanced cyclones system for palm wasted induced flue gas was performed using both Stairmand's mathematical model and CFD simulation. As the inlet velocity increases, the collection efficiency increases regardless of the particle sizes. While the results obtained from CFD simulation are in good agreement with that of the mathematical model, a slight deviation in values was considered to be due to the assumption of non-collision between particle-to-wall, and particle-to-particle in CFD simulation.

During the simulation of serial-configured cyclones, a high range of inlet velocities was recorded for the inlet ducting design with the absence of partition. Such a high inlet velocity was deemed to be undesired due to potential high erosion wear of the internal wall of the cyclone. With the addition of partition in the design of the inlet ducting, more uniformly distributed flow was observed in the outlet ducting, but the formation of undesired vortex was also evident. The formation of vortex at the outlet ducting was able to minimize with the change of shape of the outlet ducting from tapered to rectangular, by keeping the same design of the inlet ducting with partition. The use of the newly designed outlet ducting of rectangular shape also produces the desired pressure gradient with the presence of negative draft along the outlet ducting.

Acknowledgements

The authors would like to thank INTI International University for the facility support, and the Boilermech Sdn. Bhd. for the opportunity for this project collaboration.

Reference

[1] Ontko J. Similitude in cyclone separators. Powder Technology, 2016;289: 159-162.
[2] Gimbun J, Chuah T, Choong T, and Fakhru'l-Razi A. Prediction of the effects of cone tip diameter on the cyclone performance. Journal of Aerosol Science, 2005; 36(8): 1056-1065.
[3] Fu P, Wang F, Yang X, Ma L, Cui X, and Wang H. Inlet Particle-Sorting Cyclone for the Enhancement of PM2.5 Separation. Environmental Science & Technology, 2017; 51(3): 1587-1594.
[4] Heumann W. Industrial air pollution control systems. 1st ed. New York: McGraw-Hill 1997: 305-366.
[5] Safikhani H, and Mehrabian P. Numerical study of flow field in new cyclone separators. Advanced Powder Technology, 2016; 27(2): 379-387.
[6] Wan G, Sun G, Xue X, and Shi M. Solids concentration simulation of different size particles in a cyclone separator. Powder Technology, 2008; 183(1): 94-104.

[7] Azadi M, and Azadi M. An analytical study of the effect of inlet velocity on the cyclone performance using mathematical models. Powder Technology, 2012; 217: 121-127.
[8] Oriaku EC, Agulanna CN, Edeh CJ, and Adiele ID.Correlation Between Entry Velocity, Pressure Drop and Collection Efficiency in a Designed Stairmands Cyclone. American Journal of Research, 2014; 3(6): 120-126.
[9] Lede J, Li H, Soulignac F, and Villermaux J. Measurement of solid particle residence time in a cyclone reactor: A comparison of four methods. Chemical Engineering and Processing: Process Intensification, 1987; 22(4): 215-222.
[10] Shalaby H, Wozniak K, and Wozniak G. Numerical Calculation of Particle-Laden Cyclone Separator Flow Using Les. Engineering Applications of Computational Fluid Mechanics, 2008; 2(4): 382-392.
[11] Baltrenas P, Pranskevicius M, and Venslovas A. Optimization of the New Generation Multichannel Cyclone Cleaning Efficiency. Energy Procedia, 2015; 72: 188-195.
[12] Utikar R, Darmawan N, Tade M, Li Q, Evans G, Glenny M, and Pareek V. Hydrodynamic Simulation of Cyclone Separators. Computational Fluid Dynamics. in H. W. Oh (ed.), Computational Fluid Dynamics, IntechOpen, London. 10.5772/7106.
[13] Huang Y, Mo X, Yang H, Zhang M, and Lv J. Effects of Cyclone Structures on the Pressure Drop Across Different Sections in Cyclone Under Gas–Solid Flow. Clean Coal Technology and Sustainable Development,2016; 301-307.
[14] El-Batsh H. Improving cyclone performance by proper selection of the exit pipe. Applied Mathematical Modelling, 2013; 37(7): 5286-5303.
[15] Barth W. Design and layout of the cyclone separator on the basis of new investigations. Brennstoff Kraft (BWK), 1956; 8: 1.
[16] Dietz PW. Collection efficiency of cyclone separators. AIChE Journal, 1981; 27(6): 888-892.
[17] Coker, A. K. (1993) Understand cyclone design. Chemical Engineering Progress, 28, 51-55.
[18] Mothes H. Prediction removal in cyclone separators. Int. Chem. Engng.,1988; 28: 231-240
[19] Chen J, & Shi M. Analysis on cyclone collection efficiencies at high temperatures. China Particuology, 2003; 1(1): 20-26.
[20] Moore M, and McFarland A. Design of Stairmand-Type Sampling Cyclones. American Industrial Hygiene Association Journal, 1990; 51(3): 151-159.
[21] Gopani N, and Bhargava A. Design of High Efficiency Cyclone for Tiny Cement Industry. International Journal of Environmental Science and Development, 2011; 350-354.
[22] Elsayed K, and Lacor C. The effect of cyclone inlet dimensions on the flow pattern and performance. Applied Mathematical Modelling, 2011; 35(4): 1952-1968.
[23] Jianping W. The gas-solid flow characteristics of cyclones. Powder Technology, 2016; 308: 178-192.
[24] Gabitto J, and Tsouris C. Drag coefficient and settling velocity for particles of cylindrical shape. Powder Technology, 2008; 183(2): 314-322.
[25] Dirgo J, Leith D., (Ed.) Encyclopedia of fluid mechanics, 1986; Vols. 4. Houston: Gulf Publishing Company.

To whom correspondence should be addressed: Dr. Girma T. Chala, International College of Engineering and Management, P.O. Box 2511, C.P.O Seeb 111, Muscat, Oman; e-mail: girma@icem.edu.om